Industrial Combustion Symposium, Greenville SC 2022

A volume of fluid approach to model injection of highly viscous fluids

A. Ceschin*, P. Guida, C. Canciani, S. R. Gubba, S. Saxena, W. L. Roberts and H. G. Im
Clean Combustion Research Center
King Abdullah University of Science and Technology
Thuwal 23955, Saudi Arabia

Abstract

Despite the transition to renewable energy sources, fossil fuels will still play a significant role in satisfying the world's energy needs shortly. In addition, the rise in the demand for light distillates and the depletion of light crude oil reservoirs are shifting the interest toward the conversion of heavy fuel oils. The gasification process converts solid or liquid organic mixtures into lighter and cleaner components. Liquids gasification is often performed in entrained-flow gasifiers: a spray is injected from the top into an oxidizing environment in these reactors. One of the significant challenges of gasification of a liquid feed is to achieve adequate atomization, which results in increased yield of the process and minimization of solid residue formation. Both phase change and reactivity of the liquid are proportional to the surface exposed to the hot oxidizing environment. In this context, it is crucial to model the injection process. The fuels processed in gasification reactors consist of heavy and generally viscous mixtures. The peculiar physical properties of those fuels need to be adequately modelled in CFD simulations of the injection. This work demonstrates the application of the volume of fluid (VoF) method to simulate injection in an entrained-flow gasifier. The VoF allows capturing the interface between liquid and gas through a variable, called volume fraction, which is the non dimensional volume of one phase in the computational cell in the grid. The software adopted for the simulations is based on the OpenFOAM library. It combines a series of state-of-the-art techniques to address the difficulties of the problem in the framework of finite volume large eddy simulations. The volume fraction of liquid is advected geometrically using the isoAdvector algorithm with piecewise linear interface construction (PLIC) to accurately resolve ligaments down to small droplets. The latter is essential for accurate curvature estimation. Adaptive grid refinement (AGR) helps this purpose. Also, a transition of smaller droplet to Lagrangian particles unlocks large-scale simulations while optimizing computational cost. The physical properties were assumed to be constant, not a function of the liquid temperature pressure or concentration, since the injection is a relatively short phenomena confined to few diameters downstream the nozzle. The same assumptions would not be valid outside the considered region. The goal of the work in progress is to identify the proper injection mechanism and highlight which Sauter mean diameter distribution would be best to set up proper inlet boundary conditions in a reduced-order gasifier model.

*Corresponding Author: alberto.ceschin@kaust.edu.sa

1 Introduction

The steep increase in the world's energy demand cannot be satisfied in the foreseeable future by renewable energy alone, despite the significant development in recent years. Therefore, the energy market will still heavily depend on fossil fuels, whose environmental impact must be reduced. Together with this aspect, the constant depletion of light crude oil reservoirs is pushing towards the exploitation of heavier crude oils, that produce a larger amount of heavy fuel oils (HFOs) [1]. Their combustion has a significant impact on pollution [2], so it is fundamental to find ways to reduce the environmental footprint deriving from the exploitation of this energy source. The gasification process is a promising alternative to convert HFOs into lighter and cleaner components. Entrained-flow gasifiers are widely used to treat liquid feedstocks, by spraying them from the top of the reactor in an oxidizing environment. Adequate atomization in the inlet section is a crucial step to obtain a homogeneous droplet size distribution in the equipment, that increases process yield and reduces pollutant formation. HFOs, in fact, tend to form solid residues [3] as a result of liquid phase pyrolysis. Qauntitative data of the amount of surface area are needed to extimate the extent of its reactivity and its phase change. To this scope, understanding of the atomization process is a key aspect.

In this background, CFD simulations are a useful tool to understand the behavior of HFO sprays in a variety of conditions. The main challenge to overcome, in detail, is the high viscosity of HFOs, that reduces the degree of atomization. Indeed, the present work target a liquid fluid of $180cSt$, about two order of magnitude higher than water. In addition, solid particles and harsh operating conditions may represent an additional obstacles, that is why simple configuration exploiting swirl motion ([4]) or coaxial shear layers are preferred to moving parts (rotary atomizers). Despite numerous works on air-blast atomization, few of them have been performed at high pressure and for high viscous fluid [5, 6].

In the end, the common target is to avoid larger droplet and so poor conversion. From this point of view, smaller droplets become negligible since are not the bottle neck of the process. Hence the idea to perform Large Eddy Simulation in the present work.

2 Case study: coaxial air-blast atomizer

The geometry of the numerical experiment is depicted in Figure 1. Axial direction is top to bottom, since the liquid is injected from the top into the oxidizing environment of the gasifier, and falls due to gravity until the bottom of the unit, where the residue is collected. Green patch is the liquid inlet, detached from the surrounded air inlet patch (red) by a $0.1mm$ wall. Nozzle walls are blue and finally far-field is yellow. The choice of a straight nozzle was made for sake of simplification. On the other side, since PLIC-RDF is combined with dynamic grid refinement, a box spray chamber is preferred to a cylindrical one. Moreover, the code used incompressible and there is no acoustic issue of asymmetric wave reflections at walls. The present configuration targets about $15kg/hr$ of vacuum residue. Therefore, assuming a reasonable nozzle diameter of $2mm$, flow velocity results in $1.4m/s$ and therefore the flow is expected to be laminar. Viscosity is high ($180cSt$), resulting Reynolds number is about 8. Differently, the gas phase needs enough shear to break the liquid jet. Therefore, once the gas inlet velocity is constrain to $60m/s$ (for neglecting compressibility effects), and the gas to liquid ratio fixed at 0.75, the inlet air patch results in about $7.6mm^2$ surface. Dimensions of the geometry are summarized in table 1 and operative conditions in tab. 2.

Length	Value
Diameter of the liquid fuel inlet patch	2
Gap between liquid and gas patches	0.1
Internal diameter of the air inlet patch	2.2
External diameter of the air inlet patch	3.82
Nozzle length	10
Width of the spray chamber	30
Length of the spray chamber	60

Table 1. Lengths of the geometry. Units are millimeters

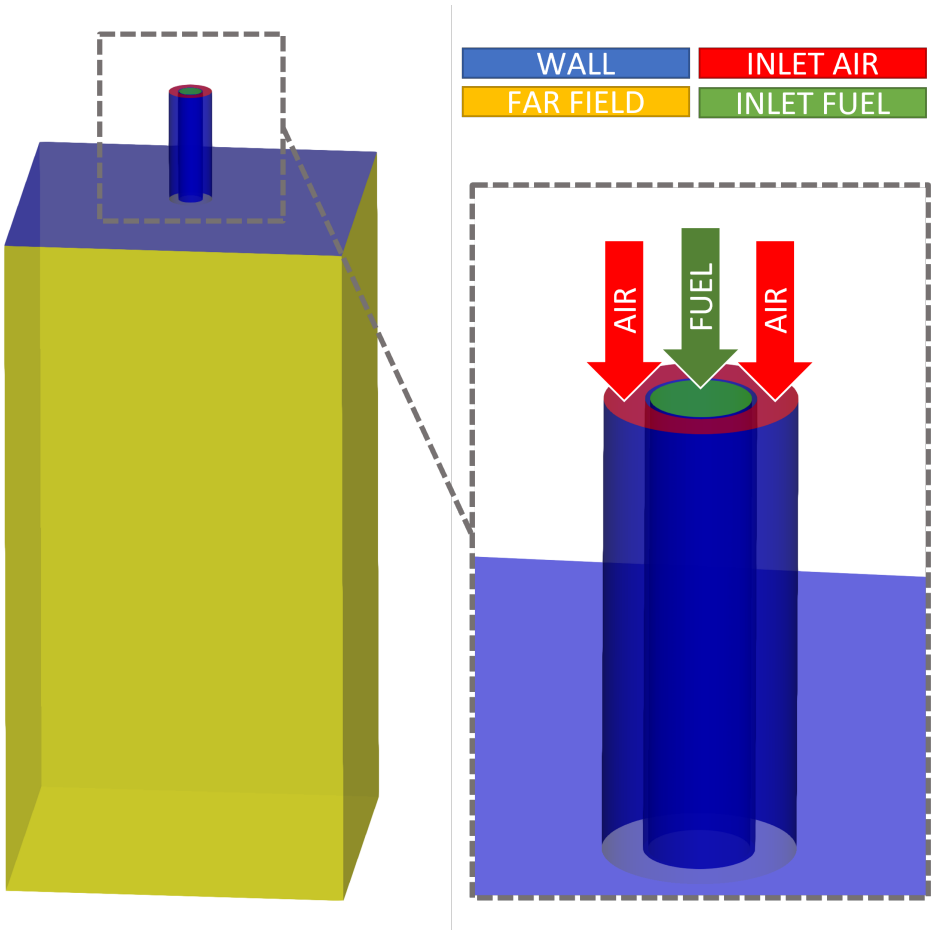

Figure 1. Configuration of the geometry. Injection happens from the patches at the top.

3 Numerical model

Incompressible LES

As previously stated, the configuration has been designed to limit the air flow to the incompressible regime ($Mach < 0.3$). Moreover, to further reduce computational cost, impact of smallest isotropic scales has been modeled by Large Eddy Simulation (LES) [7]. Therefore, descriptive equations for the filtered quantities are:

$$\nabla \tilde{u}_j = 0 \tag{1}$$

$$\frac{\partial(\bar{\rho}\widetilde{u}_i)}{\partial t} + \frac{\partial(\bar{\rho}\widetilde{u}_i\widetilde{u}_j)}{\partial x_j} = -\frac{\partial \bar{p}}{\partial x_i} + \frac{\partial}{\partial x_j}(2\bar{\mu}\widetilde{S}_{ij}) + \frac{\partial L_{ij}}{\partial x_j}, \tag{2}$$

and the stress tensor is defined as

$$\widetilde{S}_{ij} = \frac{1}{2}\left(\frac{\partial \widetilde{u}_i}{\partial x_j} + \frac{\partial \widetilde{u}_j}{\partial x_i}\right) - \frac{1}{3}\delta_{ij}\frac{\partial \widetilde{u}_k}{\partial x_k}. \tag{3}$$

Eq. 1 represents the conservation of mass and eq. 2 the conservation of momentum. Furthermore, the $\bar{}$ symbol represents filtered quantities, while the $\widetilde{}$ symbol represents density-weighted (Favre) filtered quantities. In the above equations, ρ is the density, u_j is the velocity in direction j, p is the pressure, τ_{ij}^{tot} is the total stress tensor, and δ_{ij} is the Dirac delta. The subgrid scale stress tensor, L_{ij}, must be modeled. According to the eddy viscosity assumption, it is expressed as

$$L_{ij} = \widetilde{u_i}\widetilde{u_j} - \widetilde{u_i}\widetilde{u_j} \sim 2\nu_t\widetilde{S}_{ij}\,, \tag{4}$$

Parameter	Liquid HFO	Air	Unit
Mean velocity	1.4	60	m/s
Nozzle cross area	3.14	7.65	mm^2
Density	962	7	kg/m^3
Flowrate	15.2	11.6	kg/s
Gas to liquid ratio	0.76	-	-
Viscosity	173	0.124	$mPa \cdot s$
Characteristic length	1	1.91	mm
Surface tension	32	-	mN/m
Pressure	6	-	bar
Temperature	323	323	K
Reynolds	8	6,400	-
Weber	117	-	-

Table 2. Target operative conditions. Non-dimensional numbers have been evaluated on the nozzle radii.

where ν_t is the turbulent viscosity, which also requires a model. For this work, the wall-adapting local eddy-viscosity (WALE) [8] model is suitable to achieve flow turbulence transition at the walls and adequate on not uniform grids. This model is based on the construction of tensor invariant $\mathcal{S}_{ij}^d$ and models the turbulent viscosity as

$$\nu_t = (C_w \Delta)^2 \frac{(\mathcal{S}_{ij}^d \mathcal{S}_{ij}^d)^{3/2}}{(\widetilde{S}_{ij} \widetilde{S}_{ij})^{5/2} + (\mathcal{S}_{ij}^d \mathcal{S}_{ij}^d)^{5/4}}\,, \tag{5}$$

where C_w is a constant by assuming that the model gives the same ensemble-average subgrid kinetic energy dissipation as the classical Smagorinsky model.

Volume of Fluid method

To capture the interface between the two phases, the VoF method was used. Eq. 6 represents the advection of the liquid fraction (α):

$$\frac{\partial \alpha}{\partial t} + \nabla \cdot (\alpha \mathbf{u}) = 0 \tag{6}$$

and it is solved geometrically by the isoAdvector approach [9], once the interface has been reconstructed by the plic-RDF algorithm [10]. The framework has been shown to be more accurate than other previously implemented algebraic method (MULES) in the OpenFOAM library [11]. Once the value of α field is known, density and viscosity can be estimated as a volume-based average between liquid and gas in each computational cell.

Boundary conditions

Due to the high-Reynolds regime of the air flow inside the duct, special care was adopted to this portion of the domain. In a separate mesh and before the run time, with no liquid duct or spray chamber, it was verified the gas flow transitioned to turbulent, exploiting mapped boundary conditions to a section 4 diameters downstream. Once the transient was overcome, the result was mapped to the domain in fig. 1 and the liquid injected. Again, also mapped boundary conditions were used for the the inlet patch of the liquid phase. Since velocity is imposed at the inlet, a total pressure ($6bar$) boundary condition was set at the outlet (far field); finally,walls are no-slip for the velocity field. To minimise impact of outlet boundary conditions, the computational domain extends to 30 and 8 nozzle diameters in the axial and radial directions, respectively.

Computational domain and meshing strategy

The snappyHexMesh toolbox was found suitable to mesh the geometry that was generated on Salome [12]. The starting grid has 1.5M cells, mostly regular hexahedra, with an exception for the nozzle walls due to the curvature constrain. To capture most significant liquid ligaments and velocity scaling near the walls, up to 6 levels of refinement are used at the interface and near the walls. Since the most coarse grid is about $2mm$ in resolution, the maximum resolution reached is below $30\mu m$. If wall refinement is a static

procedure, interface refinement is performed at run time and requires adequate cure. Fig. 2 clearly shows the intended strategy. Since PLIC-RDF is used, more cells are needed to be refined upstream and downstream the interface to better capture its curvature; therefore, the original code has been improved to extend the number of refined cells in the direction perpendicular to the interface.

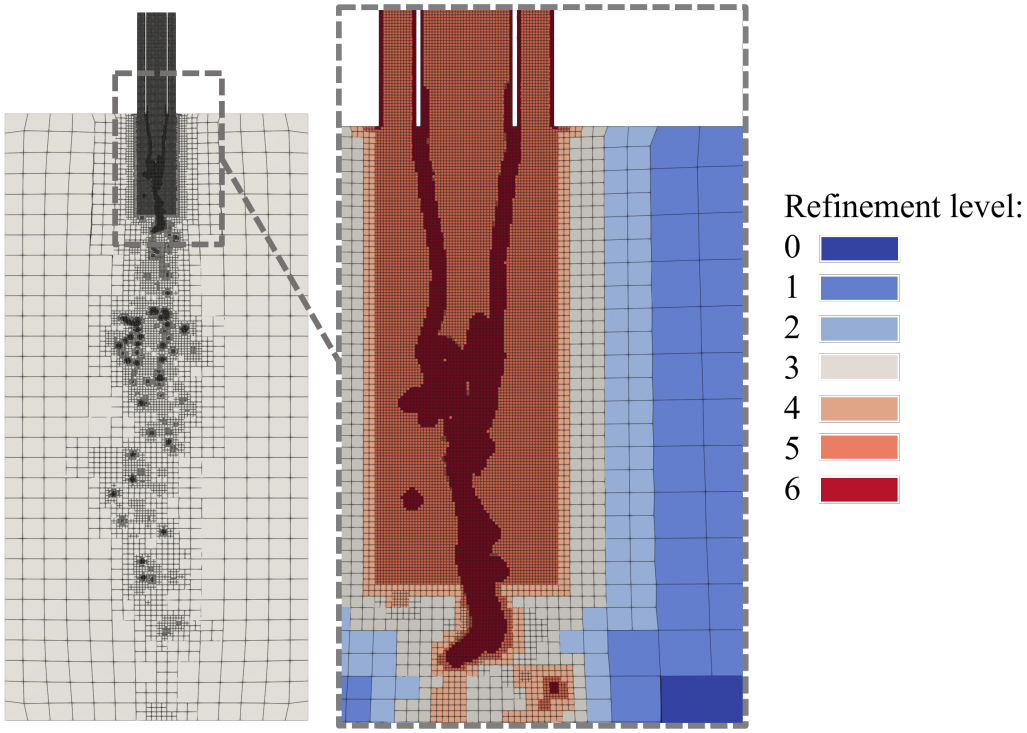

Figure 2. Longitudinal 2D cut of the computational grid: static and dynamic refinements are showcased. Ducts and primary break up region are statically refined to 5 levels, whereas walls and gas-liquid interface to 6.

Lagrangian coupling

Since Weber number is well beyond its critical value, jet and droplet break up are expected to happen. Smaller satellites droplet can form during these phenomena, and these entities may have a resolution finer than the grid. The computational cost to fully resolve these would simply be prohibitive. Therefore, the present work is focused on the primary breakup, and each droplet that falls inside a "2 grid cells" diameters criteria is removed from the domain and a Lagrangian particle is injected with the corresponding momentum. In this way, the grid can be unrefined locally and the effort focused on other portions of the domain. This approach is further motivated by the fact that the faster gas easily entertain the smallest droplets and push them away from the primary break up region. Downstream, the regime is disperse, so no droplet interaction or coalescence is needed as first degree of approximation. Nevertheless, droplet are modelled as simple spheres, so a drag contribution from the Lagrangian field to the Eulerian gas flow was taken in account. Coupling criteria between the two framework (Eulerian and Lagrangian) and code implementation started from [13]. Nevertheless, the present work makes use of the PLIC-RDF data available at run time, instead of evaluating a new level set (LS) field. In detail, together with a maximum two diameters resolution, a sphericity criteria (< 2) was used to switch from an Eulerian droplet to a Lagrangian sphere. These two criteria are checked, before the PIMPLE loop and the automatic grid refinement procedure, and every 10 time steps to reduce computational costs.

Numerics

The solver used is called *interIsoFoam*. 2 outer and 3 inner correctors were used to couple solution variables inside the PIMPLE loop. In addition, at every refinement, obtained fluxed are checked to be still divergence free. To have appropriate levels of temporal resolution and accuracy, the time step was kept fixed to $1.5e-7$, corresponding to a maximum Courant number of 0.4 in the computational domain. In addition, second order resolution schemes were used for spatial discretisation of the equations, whereas only first order (implicit Euler) for time integration due to additional complexity of dynamic refinement. Gradient and divergence terms were evaluated with linear interpolation; Sweby limiter was applied to avoid oscillation. The set-up is very efficient, and only about 35k core hours were used in this exploration work.

4 Results

For air-blast atomizer, usually two main break up regimes are expected -if the outer flow is turbulent and the inner flow laminar- and they happen according to the surrounding gas velocity [14]. In detail, the first is the bag mode, happening for lower gas velocity. The entire jet oscillates side to side at lower frequencies and the gas penetrates the liquid core, forming bags that collapse once the liquid film is too thin. This mode was present in the simulation only during the initial transient, and it is depicted on the bottom part of fig. 3 (Mode I). Unfortunately, one of the limitation of the VoF method is the impossibility

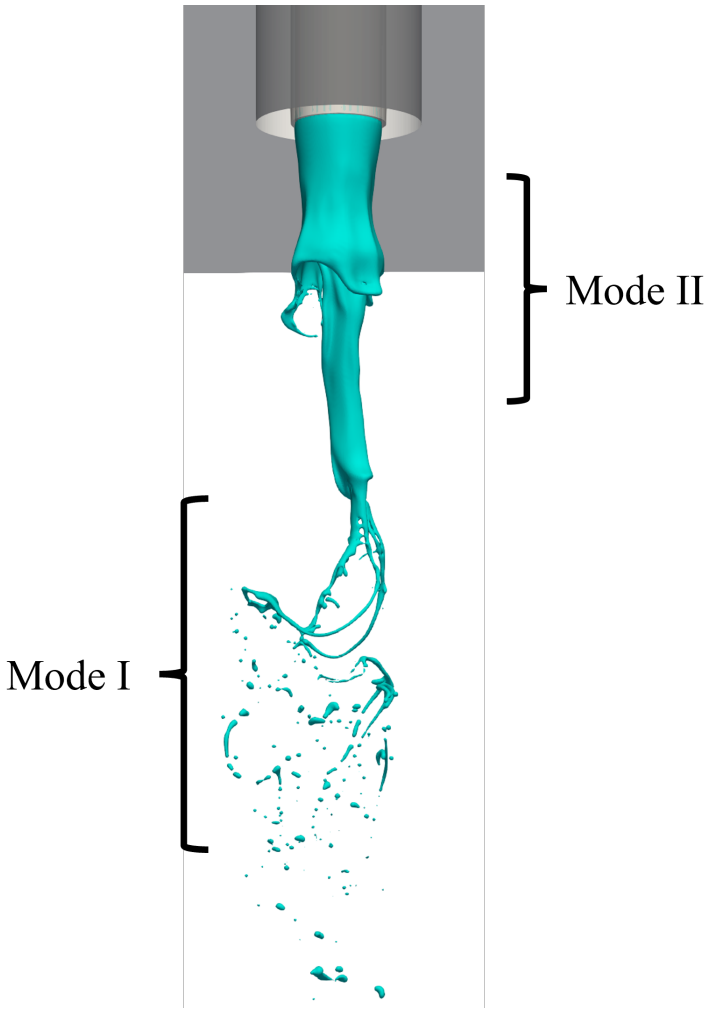

Figure 3. Liquid jet, initial transient. On the bottom the first mode, bag break-up, is identified. On the top section, the characteristic mode of the configuration, consisting in the coaxial gas peeling off the most exterior surface of the liquid.

to capture a liquid film once it gets thinner than the grid resolution. Therefore, this mode can not be properly reproduced in the current framework, unless expensive direct numerical simulation (DNS) is used. Nevertheless, liquid ligaments, marking the the bag edges, are evident. Very long liquid ligaments are also typical of viscous liquid. As a side note, few attempts to overcome this VoF limitation have been recently done in literature [15, 16]. The second mode for air-blast atomizers happens once the air velocity overcomes a certain threshold, and the jet stops oscillating side to side. In detail, the exterior part of the liquid jet is peeled off, all at the same time and all around, by the gas co-flow. Liquid instabilities form around a precise frequency, accelerating and growing downstream, until collapse happens (fig. 3). Larger harpoons are then distinguishable also inside the downstream droplets cloud. This process is clear in the sequence of snaps in fig. 4. Here, snaps are divided by $1ms$ each other. This is the characteristic dynamics governing the present configuration (top part of figure 3) and, interestingly, begins only after the initial transient. To understand

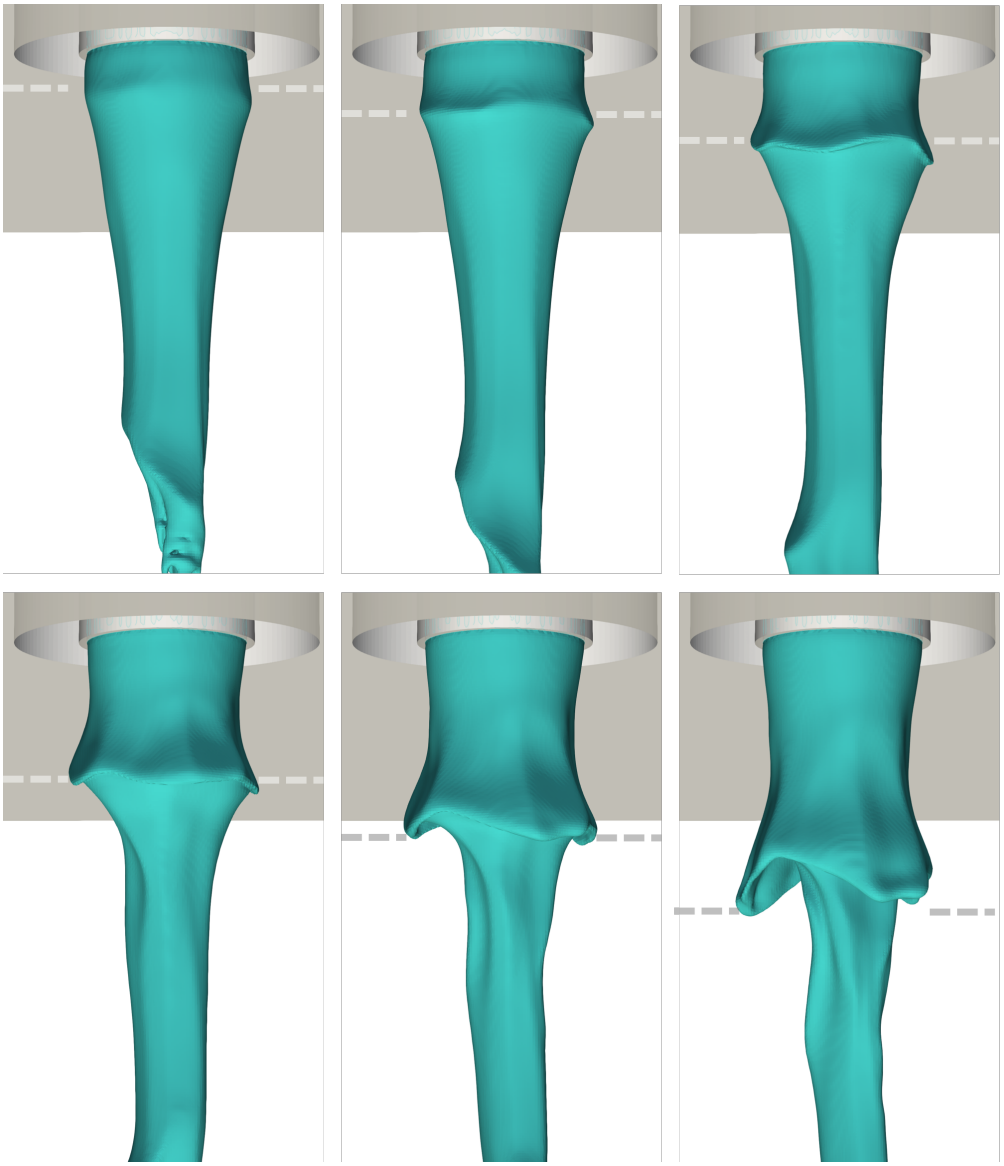

Figure 4. Liquid jet at the nozzle exit, side view. 8 different times, each $1ms$. The coaxial air flow peels off the liquid at the interface, growing the instability. A dashed line was added to track the acceleration of the wave. The next time is in fig. 3

.

the physics behind, axial velocity isocontour can be analyzed in fig. 5. Low pressure torus all around the jet are highlighted by white circles and the resulting pulling forces of the gas on the liquid by the arrows.

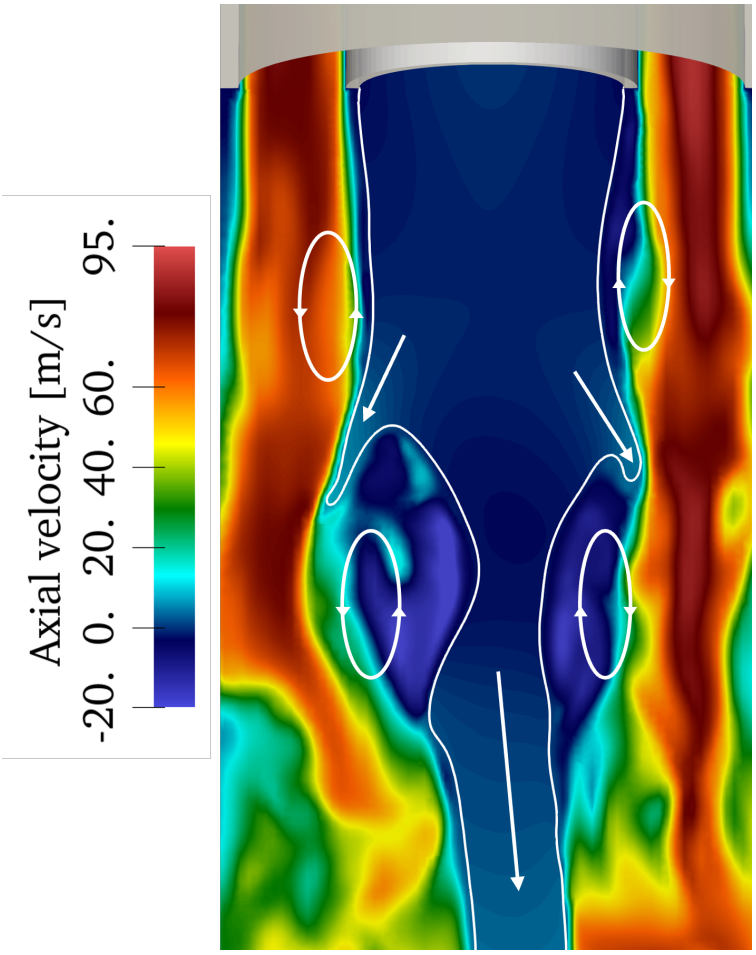

Figure 5. 2D cut showing the axial velocity isocontour. Positive velocity is top to bottom, according to the main flow direction. Re-circulation torus and velocity gradients are highlighted with white arrow to showcase the fores acting on the liquid jet. Interface ($\alpha = 0.5$) is the continuous white line.

Droplets near the far field

Fig. 6 represents the droplet population in the near outlet region. Only a few bigger droplets of maximum half millimetres have been detected in the whole simulation in this region. Of which, some are still unstable and oscillating, therefore encountering further secondary break-up. But the most are in equilibrium and the relative velocity with the liquid has almost reached to zero.

5 Conclusion

We successfully performed a Large Eddy Simulation of the primary breakup of a viscous liquid jet surrounded by a coaxial gas stream. Results will be validated when experiments on a similar configuration will be available. Nevertheless, the jet behaves as expected from a literature search. The main mechanism is the peeling of the most exterior part of the liquid jet, performed by the coaxial gas. Surface waves grow, accelerate and eventually collapse. Due to the extremely high viscosity, long liquid ligaments are found, typical of high Ohnesorge regimes.

Acknowledgments

The work was sponsored by the Clean Combustion Research Center at King Abdullah University of Science and Technology (KAUST). Computational resources were provided by the KAUST Supercomputing

Laboratory (KSL).

References

[1] BP Energy Outlook. *London, United Kingdom2019*, 2019.

[2] Abdul Gani Abdul Jameel, Abdulrahman Alkhateeb, Selvedin Telalović, Ayman M. Elbaz, William L. Roberts, and S. Mani Sarathy. In K. Murali, V. Sriram, Abdus Samad, and Nilanjan Saha, editors, *Proceedings of the Fourth International Conference in Ocean Engineering (ICOE2018)*, pp. 1047–1055, Singapore, 2019. Springer Singapore.

[3] Long Jiang, Ayman M. Elbaz, Paolo Guida, Saeed Mohammed Al-Noman, Ibrahim A. AlGhamdi, Saumitra Saxena, and William L. Roberts. *Energy & Fuels*, 33(2):1570–1581, 2019.

[4] E Laurila, J Roenby, V Maakala, P Peltonen, H Kahila, and V Vuorinen. *International Journal of Multiphase Flow*, 113:371–388, 2019.

[5] Feichi Zhang, Thomas Müller, Thorsten Zirwes, Simon Wachter, Tobias Jakobs, Peter Habisreuther, Nikolaos Zarzalis, Dimosthenis Trimis, and Thomas Kolb. *Conference on Liquid Atomization and Spray Systems, December*, pp. 1–8, 2019.

[6] Feichi Zhang, Thorsten Zirwes, Thomas Müller, Simon Wachter, Tobias Jakobs, Peter Habisreuther, Nikolaos Zarzalis, Dimosthenis Trimis, and Thomas Kolb. *Renewable and Sustainable Energy Reviews*, 134:110411, 2020.

[7] Stephen B Pope. Turbulent flows, 2001.

[8] F. Nicoud and F. Ducros. *Flow, Turbulence and Combustion*, 62(3):183–200, 1999.

[9] Johan Roenby, Henrik Bredmose, and Hrvoje Jasak. *Royal Society open science*, 3(11):160405, 2016.

[10] Henning Scheufler and Johan Roenby. *Journal of computational physics*, 383:1–23, 2019.

[11] Lionel Gamet, Marco Scala, Johan Roenby, Henning Scheufler, and Jean-Lou Pierson. *Computers & Fluids*, 213:104722, 2020.

[12] Aster Code. Salome-meca, 2018.

[13] Martin Heinrich and Rüdiger Schwarze. *SoftwareX*, 11:100483, 2020.

[14] Philippe Marmottant and Emmanuel Villermaux. *Journal of fluid mechanics*, 498:73–111, 2004.

[15] Leonardo Chirco, Jacob Maarek, Stéphane Popinet, and Stéphane Zaleski. *Journal of Computational Physics*, p. 111468, 2022.

[16] Robert Chiodi and Olivier Desjardins. *Journal of Computational Physics*, 449:110787, 2022.

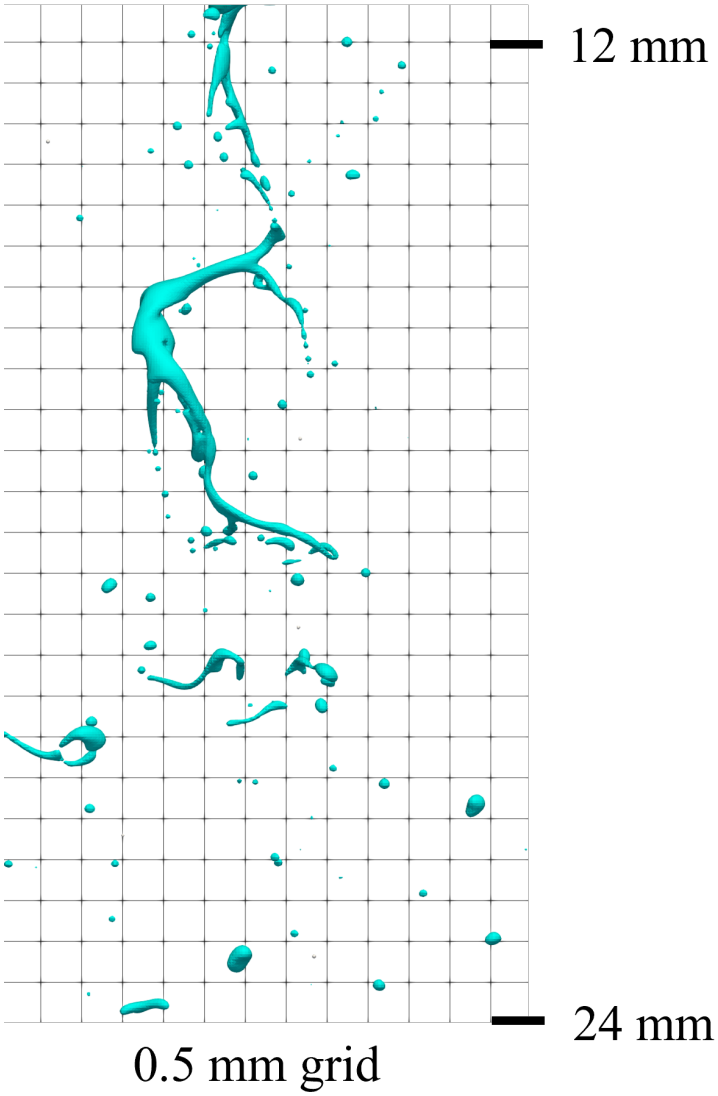

Figure 6. Portion of the domain between 12 and 24mm from the nozzle exit, side view. Liquid ligaments are undergoing secondary atomization. Background grid is 0.5mm, therefore each square is about 16*16 computational cells. Lagrangian particles are included but too small to be clearly visible.